Check for updates

View Article Online
View Journal

PCCP
Physical Chemistry Chemical Physics

Accepted Manuscript

This article can be cited before page numbers have been issued, to do this please use: M. F. C. Andrade, M. Berrens, A. Noy and T. A. Pham, *Phys. Chem. Chem. Phys.*, 2026, DOI: 10.1039/D6CP00882H.

This is an Accepted Manuscript, which has been through the Royal Society of Chemistry peer review process and has been accepted for publication.

Accepted Manuscripts are published online shortly after acceptance, before technical editing, formatting and proof reading. Using this free service, authors can make their results available to the community, in citable form, before we publish the edited article. We will replace this Accepted Manuscript with the edited and formatted Advance Article as soon as it is available.

You can find more information about Accepted Manuscripts in the Information for Authors.

Please note that technical editing may introduce minor changes to the text and/or graphics, which may alter content. The journal's standard Terms & Conditions and the Ethical guidelines still apply. In no event shall the Royal Society of Chemistry be held responsible for any errors or omissions in this Accepted Manuscript or any consequences arising from the use of any information it contains.

ROYAL SOCIETY OF CHEMISTRY

rsc.li/pccp

View Article Online
DOI: 10.1039/D6CP00882H

Journal Name

ARTICLE TYPE

Cite this: DOI: 00.0000/xxxxxxxxxx

Diameter-Dependent Multiple Proton Jumps Dictate Hydronium and Hydroxide Transport in Carbon Nanotubes

Marcos F. Calegari Andrade,[a,b‡] Margaret L. Berrens,[b] Aleksandr Noy[b], and Tuan Anh Pham[b‡]

Received Date
Accepted Date

DOI: 00.0000/xxxxxxxxxx

Nanofluidic channels impose extreme confinement on water, giving rise to unusual transport phenomena of the liquid. However, how transport of hydroxide and hydronium ions is influenced by such confinement is still not fully understood. This study employs machine learning-accelerated simulations, based on SCAN density functional, to investigate proton transfer dynamics in CNTs of varying diameters (0.8 nm to 2.8 nm). The extreme confinement of water inside 0.8 nm CNT not only enhances the probability of multiple consecutive proton jumps, but also reverses the relative diffusion coefficient of hydronium and hydroxide ions in bulk water. In CNTs with diameters larger than 0.8 nm, hydronium diffuses slightly faster than in bulk, whereas hydroxide diffusion slows because of its localization near CNT walls, hindering multiple proton jumps. This work highlights the significant impact of nanoscale confinement on proton transfer dynamics, with implications for designing nanoscale systems with controlled proton transport.

1 Introduction

The study of proton transport under nanoconfinement is a fundamental area of research in chemical physics and materials science, with significant implications in fields ranging from proton exchange membranes in fuel cells [1,2] to proton transport across biological membranes [3–5]. An improved understanding of proton transport mechanism at the nanoscale can lead to better fundamental understanding and enhanced performance of these systems, where efficient proton conduction is beneficial. The unique properties of confined spaces can alter the dynamics and solvation environment of proton defects in water, making it imperative to explore these effects in detail.

Carbon nanotubes (CNTs) have been widely used as a material platform for investigating proton transport under confinement due to their exceptional structural and electronic properties. Their high aspect ratio, simple geometry, and tunable pore sizes allow precise investigations of molecular transport phenomena [6,7]. When filled with water, CNTs create a confined environment that can significantly influence the dynamics of proton transfer [8]. Their nanoscale dimensions provide a unique platform for exploring the interplay between confinement and proton mobility, offering insights that are not readily observable in bulk systems [9] and providing a simpler and more controllable platform to better understand proton transport across biological nanochannels.

Several experimental studies have revealed remarkable proton conduction by water confined in hydrophobic 1D nanochannels. For instance, Tunuguntla and coworkers observed that hydronium ions diffused an order of magnitude faster in 0.8 nm diameter CNTs compared to bulk condition, while the confinement effect was barely noticeable in 1.5 nm diameter CNTs [10]. In addition, it was found that 1 nm-wide hydrophobic nanochannels based on metal-organic frameworks displayed near-superionic conductivity under ambient conditions [11], even though the measured proton diffusion coefficient was considerably lower than that in 0.8 nm diameter CNTs. Most recently, experiments revealed that not only the CNT geometry but also its electronic structure affect ion transport [12]. Specifically, hydronium diffusion in water-filled 0.8 nm diameter metallic CNTs was faster than in semiconducting CNTs of similar diameter. These examples point to the drastic impact of extreme confinement on proton transport, even though the atomistic mechanism of their transport is not always clear. However, to this day, no experimental measurements of hydroxide diffusion in carbon nanotubes have been made.

Complementing these experimental results, molecular simulation studies have provided valuable atomic-level insights into proton transport in CNTs. Earlier work demonstrated that water confined in carbon nanotubes forms a single-file chain that enables efficient proton hopping via the Grotthuss mechanism, thereby dramatically lowering energy barriers for proton conduc-

[a] Department of Chemistry and Biochemistry, University of California Santa Cruz, Santa Cruz, California 95064, United States.
[b] Physical and Life Sciences Directorate, Lawrence Livermore National Laboratory, Livermore, California 94550, United States.
‡ Corresponding Author(s): E-mail: mcalegar@ucsc.edu; pham16@llnl.gov

Open Access Article. Published on 08 June 2026. Downloaded on 6/17/2026 12:47:13 AM.
This article is licensed under a Creative Commons Attribution 3.0 Unported Licence.

Physical Chemistry Chemical Physics Accepted Manuscript

View Article Online
DOI: 10.1039/D6CP00882H

Open Access Article. Published on 08 June 2026. Downloaded on 6/17/2026 12:47:13 AM.
This article is licensed under a Creative Commons Attribution 3.0 Unported Licence.

Physical Chemistry Chemical Physics Accepted Manuscript

tion[13–15]. Interestingly, the simulations of Peng and coworkers[16] suggested that proton transfer across CNTs does not require pre-existing hydrated cavities, since these ions can drive the formation of proton wires inside sub-nm hydrophobic nanochannels prior their crossing. Furthermore, Li and Voth[17] demonstrated that the mere existence of a hydrated nanochannel does not necessarily imply fast proton conduction through it, and water connectivity through proton wires is key to support proton proton hopping along water chains. This and other earlier works highlights how proton transport is modulated by the hydrogen-bond network in confined media[18,19]. Besides the H-bond network and connectivity of water, quantum fluctuations of the nuclei were also shown to further enhance the diffusion rates of both H_3O^+ and OH^- along one-dimensional water networks[20,21]. Collectively, these findings demonstrate that the unique ordering and quantum behavior of water under confinement lead to markedly enhanced and, in some cases, counterintuitive proton transport behavior.

Despite these advancements, it remains unclear how extreme confinement impacts multiple proton jumps in water–the primary driver of rapid proton diffusion in aqueous systems[22]. Specifically, existing studies have largely focused on sub-nm CNTs with the single-file water configuration; neglecting confinement effect on water ion diffusion from larger nanopores. This paper addresses this knowledge gap by presenting a comprehensive investigation of proton transport in CNTs, focusing on the unique effects of extreme confinement. Here, the dynamics of water ions is described with machine learning potentials, previously used to accurately predict proton transfer in bulk [23,24] and confined water[25,26]. Our modeling framework allows adequate sampling of proton transfer dynamics at a close accuracy with electronic structure theory and with system sizes relevant to experimental conditions. We find that the relative diffusion coefficients of hydronium and hydroxide ions are reversed under such conditions, indicating a significant change in their transport dynamics. Furthermore, we show that confinement exerts a distinct influence on the transport of hydronium and hydroxide ions, suggesting that the mechanisms governing proton transfer are highly sensitive to the spatial constraints imposed by the CNTs environment.

2 Methods

2.1 Machine learning potential

The potential energy surface of water confined in CNTs was predicted using machine learning models (Deep Potential smooth edition[27,28], herein abbreviated as DP) developed in our recent studies[29,30]. This model accurately reproduces both atomic and electronic structures of bulk and confined water as predicted by the SCAN density functional[31], but at significantly reduced computational cost. In this study, atomic descriptors parsed as input to DP's neural network include all pair distances within a 6Å radius cutoff, which smoothly decay over 3Å. 3 layers-deep neural network with 120 neurons per layer was used for both the descriptor and the fitting networks. The training data of the DP models were collected via active learning[32], starting from a dataset used to train a DPMD model of pure water inside CNTs[29]. Configurations of confined water, inside CNTs with diameters ranging from 0.8 to 1.5 nm diameter, with excess or deficiency of a proton were explored with 1-ns DP molecular dynamics simulations at 330 K. SCAN DFT calculations re-evaluated the atomic forces of those configurations whose maximum deviation in atomic forces exceeded 0.1 eV/Å. DFT calculations were performed with a total of +1 or -1 total charge for systems with hydronium or hydroxide, respectively. An uniform background charge was used to keep the total charge per unit cell zero. Only atomic forces were used in the DP loss function.

2.2 Electronic structure

Electronic structure calculations employing the SCAN functional were performed using the Quantum-ESPRESSO package[33]. Wavefunctions and charge density were expanded using plane waves with energy cutoffs of 110 and 440 Ry, respectively. Norm-conserving pseudopotentials of the Troullier-Martins type[34] were used to replace explicit core-valence electron interactions. Only the gamma point of the Brillouin zone was sampled.

2.3 Molecular dynamics simulations

Molecular dynamics simulations were conducted using periodically repeated 10.6 nm-long CNTs filled with water at equilibrium density. The equilibrium density of water was estimated by minimizing the average absolute value of the stress tensor of the fluid along the CNT axial direction[29]. All simulations were performed using the LAMMPS code[35], interfaced with the DeepMD-kit package[36]. The classical equations of motion were numerically integrated using the velocity Verlet method[37] with a 0.5 fs timestep. Temperature was controlled at 330 K using a single Nosé-Hoover thermostat chain with 3 beads[38,39], and both volume and the number of particles were kept fixed throughout the simulations. The 30 K elevation from ambient temperature compensates for the overestimation of water's melting temperature predicted by the SCAN functional[40].

The axial diffusion coefficient (D_z) of water ions is computed from the Einstein relation, using the mean squared displacement of water ion's O atom along the CNT axial direction (z).

$$D_z = \lim_{t\to\infty} \frac{\langle [z(t) - z(0)]^2 \rangle}{2t} \quad (1)$$

The proton coordination number for each O atom is determined from a Voronoi tesselation, with O at the center of the Voronoi polyhedron. The H-bond is defined using the Luzar-Chandler criteria[41]. The calculation of consecutive proton jumps follows the methodology used by Chen and coworkers[22]. In this method, we count the average number of consecutive (within 0.5 ps) proton transfer events in 10-ps time intervals. Proton jumps that return to the original site within 10 ps are considered rattling and thus not included in the analysis.

3 Results and discussion

3.1 Validation of the machine learning model

The validation of the DP models was performed through a measure of DP's generalization error and by direct comparison be-

View Article Online
DOI: 10.1039/D6CP00882H

Open Access Article. Published on 08 June 2026. Downloaded on 6/17/2026 12:47:13 AM.
This article is licensed under a Creative Commons Attribution 3.0 Unported Licence.

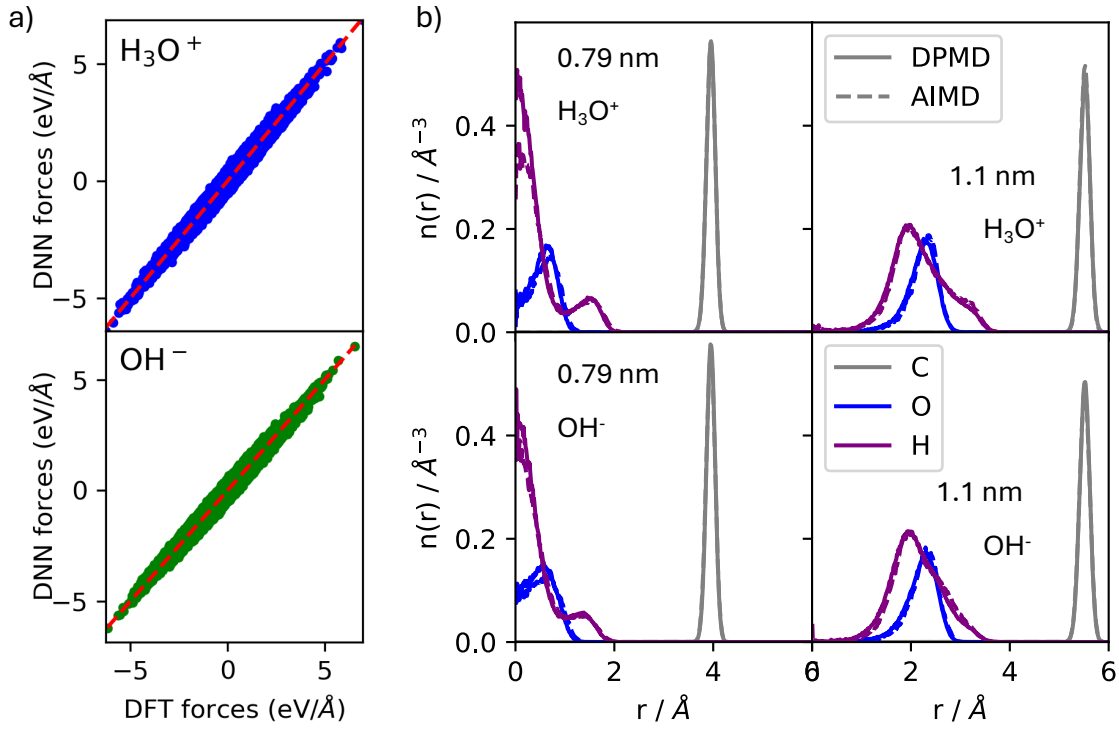

Fig. 1 a) Correlation between DFT-SCAN and DP predicted atomic forces. The forces were computed from 100 atomic configurations extracted from DPMD simulations of water confined in 2.0 nm diameter CNT at 330 K. Configurations were equally spaced within 1 ns-long trajectories and none of them were included in DP's training data. b) Comparison between the radial distribution (from the CNT axis) of the number densities of O, H and C atoms predicted by AIMD and DPMD simulations. Each panel contains results obtained with confined H_3O^+ or OH^- and CNT diamters of 0.79 nm or 1.1 nm, as labeled in each panel. Continuous and dashed lines indicate the results obtained from AIMD and DPMD, respectively.

tween DP and *ab initio* molecular dynamics (AIMD).

The generalization error of DP was accessed by direct correlation of DP and SCAN-DFT atomic forces of atomic configurations extracted from 1 ns DP molecular dynamics (DPMD) simulations at 330 K. The configurations were equally spaced in time (10 ps apart), and they contained one hydroxide or one hydronium ion in water confined by a carbon nanotube with 2.0 nm diameter. These systems were not included in the training data, and they can thus be used to properly access the generalization (or extrapolation) of the DP models trained in this work. The good agreement between the prediction of the force of DP and the DFT can be seen in the correlation plots shown in Fig. 1a. The top and bottom panels in Fig. 1a compare the DFT and DNN atomic forces on configurations containing one hydronium or hydroxide ion, respectively, inside a water-filled CNT with 2.0 nm diameter.

The accuracy of atomic forces predicted by DP reflects the close agreement of structural properties predicted by molecular dynamics using DP and SCAN. Fig. 1b contains the atomic density distributions of C, H and O atoms as a function of the distance from the CNT axis. Hydronium and hydroxide ions in water were confined within 0.79 nm and 1.1 nm CNT diameters, and molecular dynamics simulations ran for 40 ps with temperature controlled at 350 K. DP molecular dynamics (continuous lines) very closely reproduces the AIMD (dashed lines) atomic number density distributions. None of the configurations of these 4 AIMD runs were included in the training data of DP. The main purpose of the direct comparison between DP and *ab initio* molecular dynamics is to justify the appropriate fitting accuracy of the DNN model to sample the configurational space of the many-body system with the same accuracy as the potential it was trained on.

3.2 Proton transport inside carbon nanotubes

Summarized in Fig. 2, our simulations show that the diffusion behavior of solvated hydronium (H_3O^+) and hydroxide (OH^-) ions confined in CNTs deviates significantly from that in bulk water, underscoring the profound impact of nanoscale confinement on ionic mobility. Fig. 2a contains a set of cartoons representing some of the CNTs studied in this work. In the narrowest CNTs with a diameter of 0.8 nm, both ions exhibit axial diffusion coefficients that are an order of magnitude faster than those in bulk water (Fig. 2b). Notably, the predicted diffusivity of hydronium of 4.9±1 $Å^2/ps$ agrees well with the experimental value of 4.2±0.9 $Å^2/ps$, highlighting the quality of the simulation approach adopted here[42]. This remarkable enhancement in diffusion efficiency is attributed to the formation of a single-file water structure within the narrow CNT, as previously observed in simulations[18,43,44] (Fig. 2c, inset). This configuration, characterized by a fully hydrogen-bonded and ordered proton wire, facilitates direct proton transfer along the water chain, as suggested by pioneering studies of proton transport in water along proton wires[22,45–48]. The ordered nature of this proton wire enhances

Physical Chemistry Chemical Physics Accepted Manuscript

View Article Online
DOI: 10.1039/D6CP00882H

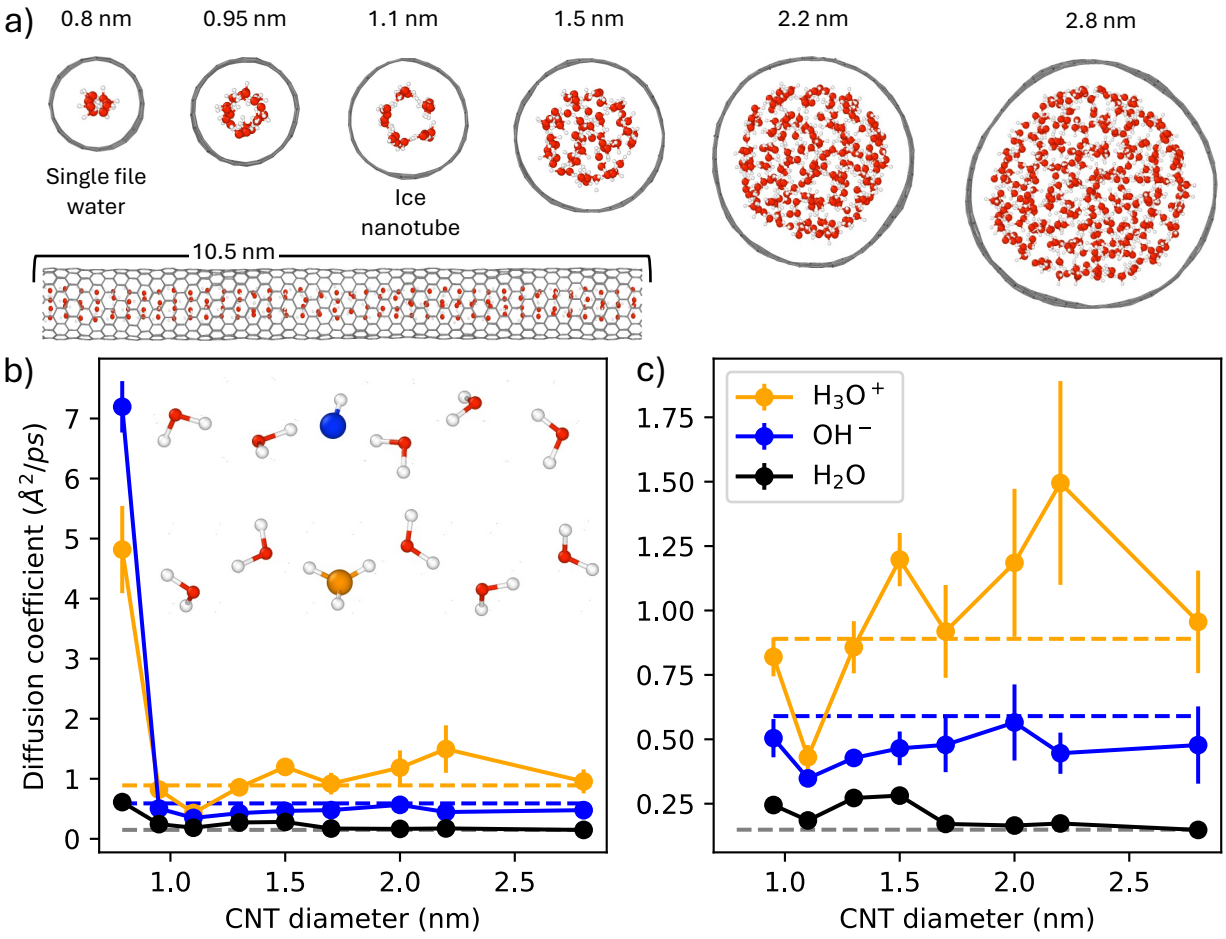

Fig. 2 a) Cross section of some of the water-filled carbon nanotubes (CNTs) studied in this work. Each simulation consists of a periodically-repeated CNT 10.6 nm in length. Labels on top of each radial cross section indicate the diameter of CNTs. b) Axial diffusion coefficient of water molecules, hydronium and hydroxide ions in water confined by carbon nanotubes with diameters ranging from 0.8 to 2.8 nm. Panel (c) contains a zoomed-in section of panel (b) with all CNTs not including the single-file water in 0.8 nm diameter CNT. Dashed lines show the diffusion coefficients of hydronium (orange) and hydroxide (blue) in bulk water. The diffusion coefficient of liquid water is shown by dashed black lines. Standard deviation is shown as a vertical line centered at each point in the graphs.

the efficiency of hydronium and hydroxide transport, leading to significantly faster diffusion rates. Most surprisingly, within this confined space, we find that hydroxide diffuses faster than hydronium, representing a reversal of the trend observed in bulk water[22].

The proton transport enhancement observed in 0.8 nm diameter CNT decays fast as the CNT diameter increases by only a few angstroms. Notably, CNTs with a 1.1 nm diameter exhibit a minimum in proton diffusion rates well below the bulk values. Slightly larger CNTs already promote the transport of hydroxide and hydronium ions with diffusion coefficients approaching those in bulk water, although from opposite angles for both water ions. These results reveal non-linear effects of hydrophobic confinement on ion diffusivity within minor variations of the confining space.

Confinement impacts not only the diffusion of water ions, but also the transport of water molecules in the absence of ions. Shown by black lines in Figs. 2b and 2c, the water diffusion coefficient surpasses the bulk water diffusion predicted by the same DP model at the same temperature (330 K). The enhancement of the water diffusion coefficient under confinement has been previously observed by *ab initio* molecular dynamics[49] and molecular dynamics performed with empirical potentials[50–53]. The fast transport of water in CNTs has been attributed to the concerted motion of the confined liquid inside the hydrophobic nanopore. For all CNTs considered in this work, proton diffusion always exceeds water diffusion, pointing to the relevance of Grotthuss diffusion on top of the vehicular motion of water ions to explain their transport properties in water.

All of the carbon nanotubes used in this work have the zigzag structure. All of these tubes are non-chiral, and thus the effect of chirality of CNTs has not been considered in our work. We note, however, that previous experimental and computational work[12] observed negligible chirality effect on hydronium transport inside semiconducting nanotubes. For this reason, our work focused exclusively on the effect of confinement on the dynamics of proton transport inside CNTs.

Open Access Article. Published on 08 June 2026. Downloaded on 6/17/2026 12:47:13 AM.
This article is licensed under a Creative Commons Attribution 3.0 Unported Licence.

Physical Chemistry Chemical Physics Accepted Manuscript

View Article Online
DOI: 10.1039/D6CP00882H

Open Access Article. Published on 08 June 2026. Downloaded on 6/17/2026 12:47:13 AM.
This article is licensed under a Creative Commons Attribution 3.0 Unported Licence.

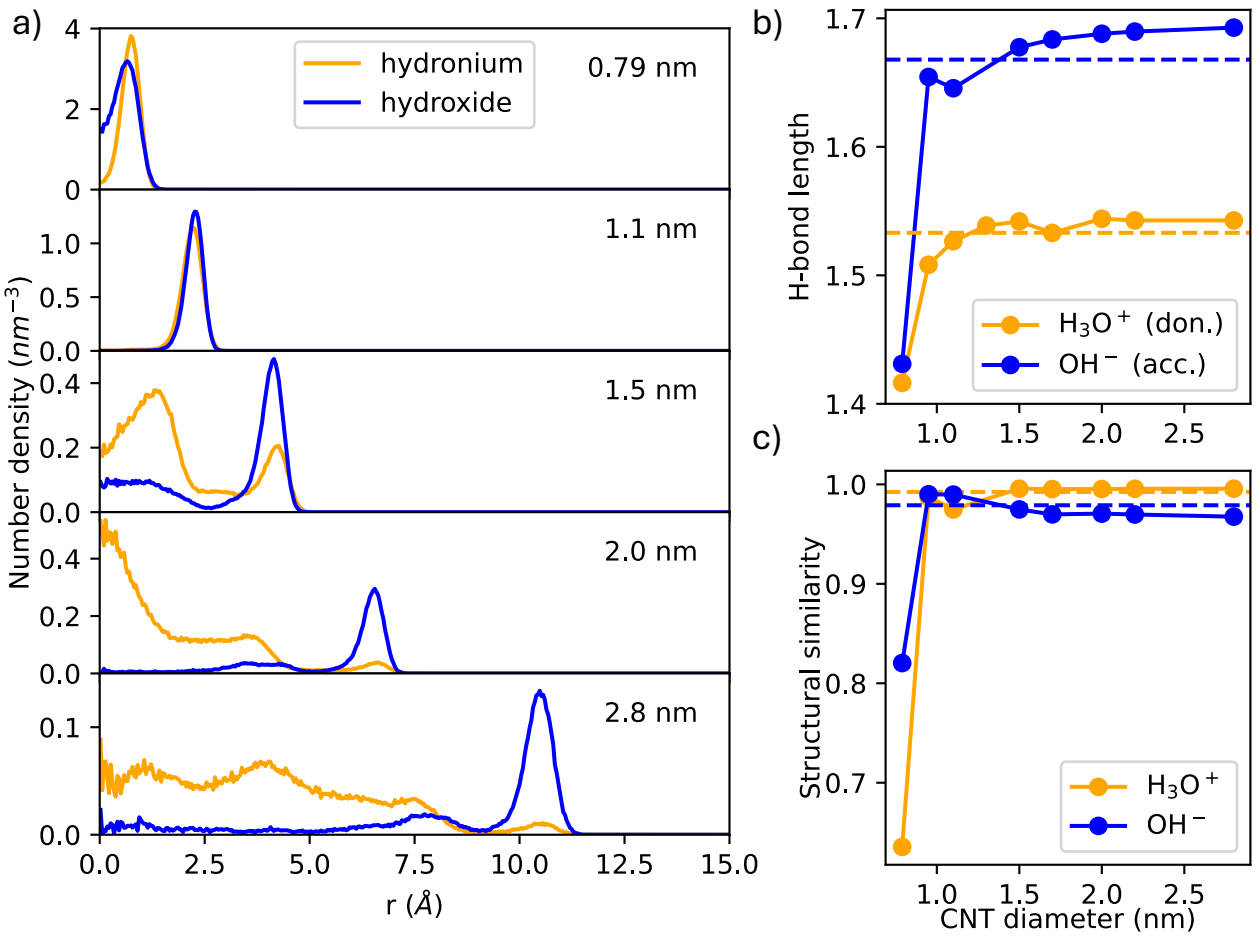

Fig. 3 a) Water-ion oxygen number density as a function of the radial distance from the CNT axis. b) Average H-bond length donated by hydronium (orange) and average H-bond length accepted by hydroxide (blue). Dashed lines indicate the average H-bond lengths of water ions in bulk water. c) Similarity of the first water solvation shell around hydronium and hydroxide relative to the first solvation shell of pure water inside the CNTs with same diameter. Dashed blue and orange lines indicate the average structural similarities of hydroxide and hydronium ions in bulk water, respectively.

3.3 The structure of the solvated proton defects in confined water

The non-linear effects of confinement on the diffusion of hydroxide and hydronium ions arise from the peculiar structures of confined water and the different solvation environment around these two ions. For instance, within a 1.1 nm diameter CNT both hydronium and hydroxide ions experience reduced mobility, which can be attributed to the formation of an ice-like water structure within the CNT, as observed in previous work[29]. This structured network, characterized by strong hydrogen bonds along the radial direction and weaker interactions axially, impedes ion movement, resulting in lower axial diffusion coefficients of the ions compared to those in bulk water or in wider CNTs. For wider CNTs (1.1 to 2.8 nm in diameter), we find that the diffusion behavior of ions begins to diverge. Specifically, hydronium ions exhibit diffusion rates slightly faster than in bulk water, indicating that even this reduced confinement can enhance mobility. In contrast, hydroxide ions diffuse more slowly than in the bulk, suggesting a very different response of the ion to the confined environment. This observation suggests that the structural and dynamic properties of water within these larger CNTs selectively influence the mobility of different ion types.

Our analysis suggests that the complex effects of hydrophobic confinement on the diffusion of hydroxide and hydronium in CNTs can be understood through the interplay of three key atomistic factors. Summarized in Fig. 3, these include: (i) spatial distribution of the ion relative to the CNT axis, (ii) H-bond geometry of the ions, specifically the lengths of accepted and donated H-bonds by the ions, and (iii) the structural similarity of the first solvation shell of water ions compared to that of confined water in the absence of ions (see SI for more details). As we discussed below, these atomic descriptors not only deepen our understanding of confinement effects on water ion transport but also provide valuable insights into the structure-dynamics relationship of these ions.

Applying the three descriptors to CNTs with a diameter of 0.8 nm reveals interesting insights about their proton transport properties. The single-file water structure in this system supports multiple proton jumps, facilitating efficient Grotthuss diffusion. In addition, the H-bond lengths donated by hydronium ions and accepted by hydroxide ions are approximately 0.3 Å shorter than their respective values in bulk water (Fig. 3b). In Grotthuss diffu-

Physical Chemistry Chemical Physics Accepted Manuscript

View Article Online
DOI: 10.1039/D6CP00882H

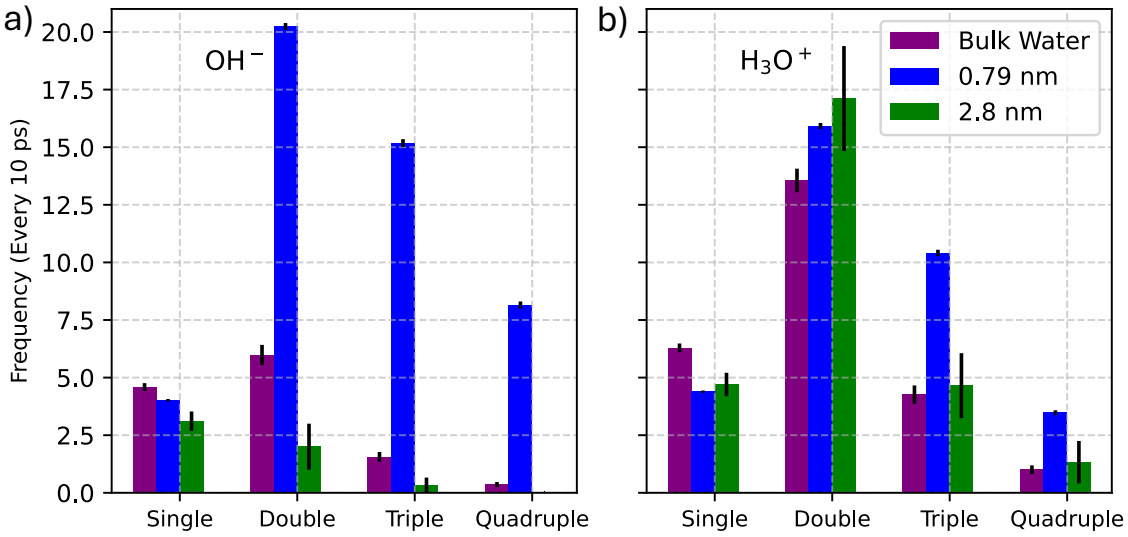

Fig. 4 Effect of 1D hydrophobic confinement on the frequency of multiple proton jumps of hydroxide (panel a) and hydronium (panel b) in water. Frequency is defined as the number of multiple proton jumps (single, double, triple or quadruple) within 10 ps of dynamics. Standard deviation is shown as a vertical line on top of each bar in the graphs.

sion, multiple proton jumps require a fully connected H-bonded and ordered water chain, whose configuration is dynamically variable in bulk water but remains intact under extreme confinement. In addition, the short H-bonds donated (accepted) by hydronium (hydroxide) place protons closer to the transition state for proton transfer. The combination of these two factors explains the faster dynamics of protons under extreme confinement relative to bulk conditions.

Besides the fast ion diffusion in single-file water, one of our key findings is the reversal of the relative diffusion rates of hydroxide and hydronium ions in 0.8 nm CNTs compared to those in bulk water (see Fig. 2b). This difference can be attributed to the orientational order of their first solvation shells relative to that of pure confined water. The closer the similarity between the solvation structure of water ions and water molecules, the lower the free energy barrier for proton transfer, thereby accelerating proton diffusion. This observation aligns with the pre-solvation mechanism of proton diffusion in water, in which solvent reorganization precedes proton diffusion–a phenomenon more evident for hydroxide ions[46]. Here, structural similarity is given by the Bhattacharyya coefficient $B(P,Q) = \int \sqrt{P(x)Q(x)}dx$, with $P(x)$ and $Q(x)$ the probability distributions of the O-O-O angle cosine (x) between a water molecule's (or water ion's) O atom and the O atoms of the nearest neighbors water molecules. $B(P,Q)$ is 0 for completely dissimilar first solvation shells of water ion and water molecules, and is 1 if their first solvation shells are identical. As shown in Fig. 3c, hydroxide ions disrupt the single-file water structure significantly less than hydronium ions, which explains their faster diffusion within the 0.8 nm diameter CNT. The small difference in the lengths of H-bonds donated by hydronium and accepted by hydroxide in this system is not sufficient to cause significant differences in proton diffusion rates (Fig. 3b).

For CNTs with a diameter of 1.1 nm, the slower diffusion of hydronium ions can be attributed to a significant distortion of their solvation environments compared to the bulk system. As shown in Fig. 3c, the structural similarity of hydronium (H_3O^+) in 1.1 nm CNT is lower than in wider CNTs. This distortion likely increases the energy barrier for proton transfer, thereby reducing the mobility of hydronium ions compared to its bulk diffusion. The same was not observed for hydroxide ions within 1.1 nm CNT diameter, and its transport rate within this level of confinement deviated much less than that of hydronium.

In CNTs with diameters larger than 1.1 nm, hydronium diffuses slightly faster than in bulk, while the opposite is observed for hydroxide ions. At this level of confinement, hydronium ions tend to localize preferentially at the core of the CNT, while hydroxide ions are predominantly found near the CNT walls. The localization of the ions as a function of the distance from the CNT axis is shown in Fig. 3a. The distribution of hydronium ions spreads out almost uniformly as the CNT diameters increases to 2.8 nm. On the other hand, the distribution of hydroxide ions always peaks near the CNT wall. This distribution is consistent with previous studies that confirm the affinity of hydroxide ions for air-water and oil-water interfaces[54,55] and the amphiphilic nature of hydroxide ions[56]. However, computer simulations have also observed higher affinity of H_3O^+ compared to OH^- to the graphene-water[57] and the air-water interfaces[58–60], pointing that both surface curvature and the underlying potential energy surface play important roles and can reverse water ion affinity to hydrophobic surfaces. The interfacial region near the CNT wall supports the hypercoordinated structure of hydroxide ions, which decreases their mobility. These spatial distribution differences and structural preferences further explain the observed differences in diffusion behavior between hydronium and hydroxide ions under varying confinement.

The bulk reference values added to Figs. 3b and 3c (dashed

Open Access Article. Published on 08 June 2026. Downloaded on 6/17/2026 12:47:13 AM.
This article is licensed under a Creative Commons Attribution 3.0 Unported Licence.

Physical Chemistry Chemical Physics Accepted Manuscript

View Article Online
DOI: 10.1039/D6CP00882H

Open Access Article. Published on 08 June 2026. Downloaded on 6/17/2026 12:47:13 AM.
This article is licensed under a Creative Commons Attribution 3.0 Unported Licence.

Physical Chemistry Chemical Physics Accepted Manuscript

lines) provide further insight into the distinct confinement response of the two ions. Both the average H-bond length and the structural similarity of hydronium converge more closely to their bulk values, as a function of CNT diameter, than those of hydroxide. This trend mirrors the spatial distribution of the ions shown in Fig. 3a: hydronium resides preferentially in the core of the CNTs, where the local environment resembles bulk water, whereas hydroxide localizes near the CNT walls and therefore experiences a local structure more distorted from bulk water than hydronium. The bulk references also reveal that the first solvation shell of hydronium is structurally more similar to that of neutral water than is the case for hydroxide. This agrees with previous simulations indicating that hydroxide ions are frequently found in a hypercoordinated state, whereas hydronium largely retains the tetrahedral local structure of neutral water molecules[46].

3.4 Proton hopping

Next, to better understand the transport mechanism of hydroxide and hydronium ions in CNTs, we analyzed the frequency of their multiple proton jumps for CNTs of 0.8 nm and 2.8 nm diameters, and compared the results to those observed in bulk water. The definition of frequency follows the one proposed by Chen and coworkers[22]. This definition counts the number of proton jumps within a 10 ps time interval excluding proton rattling between neighboring oxygen atoms. A recent study using a 100 fs time interval between consecutive jumps concluded that these events follow a Poisson distribution and are thus uncorrelated[61]. Here we adopt the original definition of Chen[22] for its usefulness in interpreting long range proton transfer in water. Our findings, summarized in Fig. 4, reveal that water ions in CNT with a 0.8 nm diameter exhibit a significantly higher frequency of single, double, triple, and quadruple proton jumps than those observed in bulk water under the same thermodynamic conditions. Notably, it is shown that the number of multiple proton jumps for hydroxide ions (Fig. 4a) is greater than that for hydronium ions (Fig. 4b), aligning with the observed faster axial diffusion coefficient of hydroxide in single-file water compared to hydronium. This observation suggests that the structural distortion of the ion solvation shells, as shown in Fig. 3c, negatively impacts correlated proton transfer along the proton wire chain. Overall, these findings suggest that solvation shell structure of hydroxide and hydronium under nanoscale confinement is a key determinant of their distinct transport behaviors in CNTs.

As a final note, for the larger 2.8 nm diameter CNT, the frequency of multiple proton jumps for hydronium ions closely resembles that observed in bulk water, consistent with the diffusion behavior of water ions in this CNT relative to the bulk system. However, hydroxide ions exhibit slightly slower diffusion in the 2.8 nm diameter CNT compared to bulk water. This behavior can be explained by the reduced number of multiple proton jumps for hydroxide ions, as these jumps are less favored near the hydrophobic interface of the CNT. Accordingly, our simulations suggest that interfacial effects also play an important role in determining ion diffusion, and that their impacts vary for different ions, depending on their solvation properties under confinement.

4 Conclusions

In conclusion, we investigated the effects of confinement on structure and dynamics of hydroxide and hydronium ions confined in CNTs, utilizing machine learning-enhanced molecular dynamics simulations. Our study reveals that transport of these ions exhibits highly non-linear confinement effects, driven by the interplay between their solvation shell structure and spatial distribution, as well as the unique hydrogen-bonding networks imposed by nano-confinement. In particular, 0.8 nm CNTs promote exceptionally fast ion diffusion by forming a single-file water chain that facilitates multiple proton jumps. Remarkably, we find that hydroxide ions diffuse faster than hydronium ions in these narrow CNTs, reversing the trend typically observed in bulk water. This faster diffusion of hydroxide is attributed to its less distorted solvation shell within the confined environment, which minimizes disruption to the single-file proton wire and enables more efficient multiple proton jumps. These findings underscore the critical role of extreme confinement in reshaping proton transfer dynamics and offer valuable insights for designing nanofluidic systems that exploit such enhanced transport properties.

Author contributions

MCA: Conceptualization, Methodology, Investigation, Writing – original draft, Writing – review & editing. MLB: Investigation, Writing – original draft, Writing – review & editing. AN: Formal analysis, Validation, Writing – original draft, Writing – review & editing. TAP: Conceptualization, Methodology, Writing – original draft, Writing – review & editing.

Conflicts of interest

There are no conflicts to declare.

Data availability

Data for this article, including the machine learning training data, DeepMD-kit input files, LAMMPS input files, initial atomic coordinates (in LAMMPS data format) and DeepMD potentials are available at `https://github.com/marcoscaa/cnt_proton_defect/tree/main`.

Acknowledgements

This work was supported as part of the Center for Enhanced Nanofluidic Transport (CENT), an Energy Frontier Research Center funded by the U.S. Department of Energy, Office of Science, Basic Energy Sciences under Award DE-SC0019112. Computational support is from the LLNL Grand Challenge Program. The work at the Lawrence Livermore National Laboratory was performed under the auspices of the U.S. Department of Energy under Contract DE-AC52-07NA27344. MCA would like to thank Ali Hassanali for providing constructive feedback on this manuscript.

Notes and references

1 G. Merle, M. Wessling and K. Nijmeijer, *Journal of Membrane Science*, 2011, **377**, 1–35.
2 Z. Long and M. E. Tuckerman, *Journal of Physical Chemistry C*, 2023, **127**, 2792–2804.

View Article Online
DOI: 10.1039/D6CP00882H

Open Access Article. Published on 08 June 2026. Downloaded on 6/17/2026 12:47:13 AM.
This article is licensed under a Creative Commons Attribution 3.0 Unported Licence.

3 J. F. Nagle and H. J. Morowitzt, *Proc. Natl. Acad. Sci. USA*, 1978, **75**, 298–302.
4 E. S. Medvedev and A. A. Stuchebrukhov, *Journal of Physics Condensed Matter*, 2011, **23**, 234103.
5 R. Pomès and B. Roux, *Biophysical Journal*, 2002, **82**, 2304–2316.
6 S. Faucher, N. Aluru, M. Z. Bazant, D. Blankschtein, A. H. Brozena, J. Cumings, J. P. D. Souza, M. Elimelech, R. Epsztein, J. T. Fourkas, A. G. Rajan, H. J. Kulik, A. Levy, A. Majumdar, C. Martin, M. McEldrew, R. P. Misra, A. Noy, T. A. Pham, M. Reed, E. Schwegler, Z. Siwy, Y. Wang and M. Strano, *Journal of Physical Chemistry C*, 2019, **123**, 21309–21326.
7 N. R. Aluru, F. Aydin, M. Z. Bazant, D. Blankschtein, A. H. Brozena, J. P. de Souza, M. Elimelech, S. Faucher, J. T. Fourkas, V. B. Koman, M. Kuehne, H. J. Kulik, H.-K. Li, Y. Li, Z. Li, A. Majumdar, J. Martis, R. P. Misra, A. Noy, T. A. Pham, H. Qu, A. Rayabharam, M. A. Reed, C. L. Ritt, E. Schwegler, Z. Siwy, M. S. Strano, Y. Wang, Y.-C. Yao, C. Zhan and Z. Zhang, *Chemical Reviews*, 2023, **123**, 2737–2831.
8 D. Muñoz-Santiburcio and D. Marx, *Chemical Reviews*, 2021, **121**, 6293–6320.
9 C. I. Lynch, S. Rao and M. S. Sansom, *Chemical Reviews*, 2020, **120**, 10298–10335.
10 R. H. Tunuguntla, Y. Zhang, R. Y. Henley, Y. C. Yao, T. A. Pham, M. Wanunu and A. Noy, *Science*, 2018, **359**, 792–796.
11 K. Otake, K. Otsubo, T. Komatsu, S. Dekura, J. M. Taylor, R. Ikeda, K. Sugimoto, A. Fujiwara, C. P. Chou, A. W. Sakti, Y. Nishimura, H. Nakai and H. Kitagawa, *Nature Communications*, 2020, **11**, 843.
12 Y. Li, Z. Li, R. P. Misra, C. Liang, A. J. Gillen, S. Zhao, J. Abdullah, T. Laurence, J. A. Fagan, N. Aluru, D. Blankschtein and A. Noy, *Nature Materials*, 2024, **23**, 1123–1130.
13 D. J. Mann and M. D. Halls, *Physical Review Letters*, 2003, **90**, 4.
14 C. Dellago, M. M. Naor and G. Hummer, *Physical Review Letters*, 2003, **90**, 4.
15 Z. Cao, Y. Peng, T. Yan, S. Li, A. Li and G. A. Voth, *Journal of the American Chemical Society*, 2010, **132**, 11395–11397.
16 Y. Peng, J. M. Swanson, S. G. Kang, R. Zhou and G. A. Voth, *Journal of Physical Chemistry B*, 2015, **119**, 9212–9218.
17 C. Li and G. A. Voth, *Proc. Natl. Acad. Sci. U. S. A.*, 2021, **118**, e2113141118.
18 J. K. Clark and S. J. Paddison, *Physical Chemistry Chemical Physics*, 2014, **16**, 17756–17769.
19 S. H. Lee and J. C. Rasaiah, *Journal of Chemical Physics*, 2013, **139**, 124507.
20 J. Chen, X. Z. Li, Q. Zhang, A. Michaelides and E. Wang, *Physical Chemistry Chemical Physics*, 2013, **15**, 6344–6349.
21 M. Rossi, M. Ceriotti and D. E. Manolopoulos, *Journal of Physical Chemistry Letters*, 2016, **7**, 3001–3007.
22 M. Chen, L. Zheng, B. Santra, H.-Y. Ko, R. A. DiStasio, M. L. Klein, R. Car and X. Wu, *Nature Chemistry*, 2018, **10**, 413–419.
23 M. C. Andrade, R. Car and A. Selloni, *Proceedings of the National Academy of Sciences of the United States of America*, 2023, **120**, e2302468120.
24 P. M. Piaggi and R. Car, *Molecular Physics*, 2021, **119**, e1916634.
25 J. Abdullah, M. C. Andrade, Z. Zhulficar, M. Berrens, Z. Li, G. Azom, Y.-C. Yao, Z. Rizer, Y. Li, S. Zhao, T. A. Pham, Y. Wang and A. Noy, *Nano Letters*, 2025, **25**, 16421–16426.
26 F. L. Thiemann, C. Schran, P. Rowe, E. A. Müller and A. Michaelides, *ACS Nano*, 2022, **16**, 10775–10782.
27 L. Zhang, J. Han, H. Wang, R. Car and W. E, *Physical Review Letters*, 2018, **120**, 143001.
28 L. Zhang, J. Han, H. Wang, W. Saidi, R. Car and W. E, Advances in Neural Information Processing Systems, 2018.
29 M. F. C. Andrade and T. A. Pham, *The Journal of Physical Chemistry Letters*, 2023, **14**, 5560–5566.
30 M. F. C. Andrade, N. R. Aluru and T. A. Pham, *Journal of Physical Chemistry Letters*, 2024, **15**, 6872–6879.
31 J. Sun, R. C. Remsing, Y. Zhang, Z. Sun, A. Ruzsinszky, H. Peng, Z. Yang, A. Paul, U. Waghmare, X. Wu *et al.*, *Nature chemistry*, 2016, **8**, 831–836.
32 L. Zhang, M. Chen, X. Wu, H. Wang, W. E and R. Car, *Physical Review B*, 2020, **102**, 041121(R).
33 P. Giannozzi, O. Andreussi, T. Brumme, O. Bunau, M. B. Nardelli, M. Calandra, R. Car, C. Cavazzoni, D. Ceresoli, M. Cococcioni, N. Colonna, I. Carnimeo, A. D. Corso, S. D. Gironcoli, P. Delugas, R. A. Distasio, A. Ferretti, A. Floris, G. Fratesi, G. Fugallo, R. Gebauer, U. Gerstmann, F. Giustino, T. Gorni, J. Jia, M. Kawamura, H. Y. Ko, A. Kokalj, E. Küçükbenli, M. Lazzeri, M. Marsili, N. Marzari, F. Mauri, N. L. Nguyen, H. V. Nguyen, A. Otero-De-La-Roza, L. Paulatto, S. Poncé, D. Rocca, R. Sabatini, B. Santra, M. Schlipf, A. P. Seitsonen, A. Smogunov, I. Timrov, T. Thonhauser, P. Umari, N. Vast, X. Wu and S. Baroni, *Journal of Physics: Condensed Matter*, 2017, **29**, 465901.
34 N. Troullier and J. L. Martins, *Physical Review B*, 1991, **43**, 1993–2006.
35 S. Plimpton, *Journal of Computational Physics*, 1995, **117**, 1–19.
36 H. Wang, L. Zhang, J. Han and W. E, *Computer Physics Communications*, 2018, **228**, 178–184.
37 M. E. Tuckerman, J. Alejandre, R. López-Rendón, A. L. Jochim and G. J. Martyna, *Journal of Physics A: Mathematical and General*, 2006, **39**, 5629–5651.
38 S. Nosé, *Molecular Physics*, 1984, **52**, 255–268.
39 W. G. Hoover, *Physical Review A*, 1985, **31**, 1695–1697.
40 P. M. Piaggi, A. Z. Panagiotopoulos, P. G. Debenedetti and R. Car, *Journal of Chemical Theory and Computation*, 2021, **17**, 3065–3077.
41 A. Luzar and D. Chandler, *Nature*, 1996, **379**, 55–57.
42 R. H. Tunuguntla, F. I. Allen, K. Kim, A. Belliveau and A. Noy, *Nature Nanotechnology*, 2016, **11**, 639–644.
43 A. Bankura and A. Chandra, *Journal of Physical Chemistry B*, 2012, **116**, 9744–9757.
44 M. L. Brewer, U. W. Schmitt and G. A. Voth, *Biophysical Jour-*

Physical Chemistry Chemical Physics Accepted Manuscript

View Article Online
DOI: 10.1039/D6CP00882H

nal, 2001, **80**, 1691–1702.

45 D. Marx, M. E. Tuckerman, J. Hutter and M. Parrinello, *Nature*, 1999, **397**, 601–604.

46 M. E. Tuckerman, D. Marx and M. Parrinello, *Nature*, 2002, **417**, 925–929.

47 C. Knight and G. A. Voth, *Accounts of Chemical Research*, 2012, **45**, 101–109.

48 A. Hassanali, F. Giberti, J. Cuny, T. D. Kühne and M. Parrinello, *Proceedings of the National Academy of Sciences*, 2013, **110**, 13723–13728.

49 G. Cicero, J. C. Grossman, E. Schwegler, F. Gygi and G. Galli, *Journal of the American Chemical Society*, 2008, **130**, 1871–1878.

50 A. Striolo, *Nano Letters*, 2006, **6**, 633–639.

51 S. Joseph and N. R. Aluru, *Nano Letters*, 2008, **8**, 452–458.

52 A. Alexiadis and S. Kassinos, *Chemical reviews*, 2008, **108**, 5014–5034.

53 T. Zhang, Z. Wang, S. Li, X. Zhang and J. Su, *Langmuir*, 2024, **40**, 27104–27113.

54 C. J. Mundy, I. F. W. Kuo, M. E. Tuckerman, H. S. Lee and D. J. Tobias, *Chemical Physics Letters*, 2009, **481**, 2–8.

55 S. Yang, M. Chen, Y. Su, J. Xu, X. Wu and C. Tian, *Physical Review Letters*, 2020, **125**, 156803.

56 Y. Crespo and A. Hassanali, *Journal of Physical Chemistry Letters*, 2015, **6**, 272–278.

57 X. R. Advincula, K. D. Fong, A. Michaelides and C. Schran, *ACS Nano*, 2025, **19**, 17728–17737.

58 M. K. Petersen, S. S. Iyengar, T. J. Day and G. A. Voth, *Journal of Physical Chemistry B*, 2004, **108**, 14804–14806.

59 Y. L. S. Tse, C. Chen, G. E. Lindberg, R. Kumar and G. A. Voth, *Journal of the American Chemical Society*, 2015, **137**, 12610–12616.

60 F. Giberti and A. A. Hassanali, *Journal of Chemical Physics*, 2017, **146**, 244703.

61 A. Gomez, W. H. Thompson and D. Laage, *Nature Chemistry*, 2024, **16**, 1838–1844.

Open Access Article. Published on 08 June 2026. Downloaded on 6/17/2026 12:47:13 AM.
This article is licensed under a Creative Commons Attribution 3.0 Unported Licence.

Physical Chemistry Chemical Physics Accepted Manuscript

View Article Online
DOI: 10.1039/D6CP00882H

Data Availability Statement

Data for this article, including the machine learning training data, DeepMD-kit input files, LAMMPS input files, initial atomic coordinates (in LAMMPS data format) and DeepMD potentials are available at https://github.com/marcoscaa/cnt_proton_defect/tree/main.

Open Access Article. Published on 08 June 2026. Downloaded on 6/17/2026 12:47:13 AM.
This article is licensed under a Creative Commons Attribution 3.0 Unported Licence.

Physical Chemistry Chemical Physics Accepted Manuscript